Desalination and Water Treatment
www.deswater.com

doi: 10.5004/dwt.2022.29056

278 (2022) 182–194
December

Comparative adsorption study of phenol removal using *Phoenix dactylifera* fiber and its chemically activated carbon

Abderrahim Khelfaoui[a,*], Noura Chaouch[b]

[a]*Process Engineering Department, Faculty of Applied Sciences, Kasdi Merbah University, 30000 Ouargla, Algeria, Tel. +213662221602; email: khe_rahim@yahoo.com*
[b]*Process Engineering Laboratory, Process Engineering Department, Faculty of Applied Sciences, Kasdi Merbah University, 30000 Ouargla, Algeria, Tel. +213776657101; Fax: +213 29 711975; email: amirchaouch@gmail.com*

Received 13 June 2022; Accepted 18 October 2022

ABSTRACT

Phoenix dactylifera waste is a burden on farm owners, the state as well as the environment, if it is not treated appropriately. Thus, to reduce this burden and its impact on the society, we have valorised these wastes by their transformation in the form of adsorbents. This study presents a comparative study of phenol removal from water solution by natural *Phoenix dactylifera* fiber (NF) and *Phoenix dactylifera* fiber chemically activated with H_3PO_4 (ACF). The sorbents were characterized by Brunauer–Emmett–Teller (BET) isotherms, Barrett–Joyner–Halenda, Fourier-transform infrared spectroscopy, X-ray diffraction and scanning electron microscopy coupled with energy-dispersive X-ray spectroscopy. NF and ACF showed a predominantly mesoporous structure with a BET surface area of 1.108 and 269.543 m^2/g, respectively. Batch adsorption experiments were carried out to study the effect of pH, contact time, adsorbent mass, initial phenol concentration and temperature on phenol adsorption. Under an optimum pH value of 6.0, the maximum adsorption capacities based on experimental results was 3.45 mg/g (with equilibrium time of 120 min) for NF, while it was 9.62 mg/g (with equilibrium time of 210 min). The adsorption isotherm of phenol on NF and ACF fits the Freundlich model well. The kinetic study showed that the adsorption data follow a pseudo-second-order kinetic model. The thermodynamic parameters namely Gibbs free energy ($\Delta G°$), standard enthalpy ($\Delta H°$) and standard entropy ($\Delta S°$) were also calculated. The results show that adsorption of phenol onto NF and ACF was non spontaneous and exothermic.

Keywords: Adsorption models; Phenol; *Phoenix dactylifera*; Activated carbon; Thermodynamics; Kinetics

1. Introduction

Phenols are widespread organic pollutants in wastewater discharges from various industries such as petroleum refineries, coal conversion, polymer synthesis, paper mills, paints, textiles plastic, rubber, insecticides and pesticides [1]. Phenolic compounds have been classified as priority pollutants by the United States Environmental Protection Agency (USEPA) and the European Union (EU). This classification is due to their toxicity and carcinogenicity properties that lead to serious impact on aquatic environment besides human and animal health [2]. According to World Health Organization (WHO) the permissible concentration of phenolic compounds in drinking water should be less than 1 μg/L. However, the USEPA requires a phenol concentration less than 1 mg/L for wastewater and 0.5 μg/L for drinking water [3].

Various physical, chemical and biological treatment procedures have been developed to remove the phenols from

* Corresponding author.

aqueous solutions such as coagulation [4], aerobic and anaerobic biological reduction [5], ozonation [6], plasma technology [7], oxidation, steam distillation and irradiation, solvent extraction, ion exchange in resins, membrane filtration, electrochemical degradation [8], reverse osmosis and adsorption onto various adsorbents [2,3]. Among all these methods, adsorption is extensively used because of its functionality costs, ease of operation, economical, adsorption capacity, availability of a wide range of adsorbent and effectiveness in removing phenols from water [9]. In recent years, several researchers have investigated different types of low-cost materials as adsorbents for remove phenol from water such as agricultural and industrial by-products [10], clay [11], sewage sludge [12], zeolites [13], fly ash [14] and polymeric resins [15].

Activated carbon (also known as activated charcoal) is a carbonaceous material, which has a porous structure and usually has a large surface area, giving it a high adsorption capacity [16]. It can be prepared from any carbonaceous material by physical and chemical activation [17]. The porosity, pore size distribution, pore shape, and surface chemistry can be affected by the nature of the precursor, activation method, and activation conditions [18]. Activated carbon prepared from agricultural and biomass wastes showed a good efficiency of removal a wide variety of organic and inorganic pollutants dissolved in aqueous medium. Tea waste [19], sawdust [20], oil palm shell, coconut shells, corn cobs, artichoke leaves, cotton stalks, pinefruit shell, jute fiber, pistachio nut shells and coffee grounds have been precursors for preparation activated carbons and their affinity towards phenols have been proved [21].

The main objectives of this research are the preparation and characterization of new adsorbents, namely natural fiber (NF) and activated carbon fiber (ACF), and the study of their efficiency in the phenol adsorption through the evaluation of different operational parameter effects, such as solution pH, contact time, adsorbent dosage, initial phenol concentrations and temperature. The obtained results of kinetic modelling and thermodynamic study ensures a thorough understanding of the adsorption phenomenon.

2. Material and methods

2.1. Preparation of adsorbents

2.1.1. Absorbent NF

The fiber of *Phoenix dactylifera* (Ghars variety) were collected from Ouargla Oasis (latitude and longitude coordinates are: 31° 57′ 9.6192″ N, 5° 20′ 0.6864″ E), located in south-east of Algeria. The fiber obtained was thoroughly washed with distilled water, dried in an oven for overnight before being crushed and sieved to desired particle size (150–250 μm).

2.1.2. Absorbent ACF

50 g of NF were soaked in 500 mL of phosphoric acid (H_3PO_4 85% purity, Sigma-Aldrich) solution (30% acid + 70 bi-distilled water) at 60°C on rotary incubator shaker for an entire day, then dried in oven for 24 h. Once activated, the carbonization was realized in muffle furnace in absence of the air at 450°C for 1 h 30 min. After that, the activated carbon was washed with distilled water until the filtrate reached to constant pH, then dried at 105°C for 24 h and finally stored in a closed container for different uses.

2.2. Characterisation of adsorbents

In this study, Brunauer–Emmett–Teller (BET) surface area, Barrett–Joyner–Halenda (BJH) pore volume and other physical parameters of adsorbents (NF and ACF) were determined on the basis of nitrogen gas adsorption–desorption using Micromeritics 3Flex adsorption analyser. The functional groups of adsorbents were identified by the Agilent Cary 640 Fourier-transform infrared spectrometer (FTIR) of Agilent Technologies at 4,000 to 400 cm^{-1} with samples pressed as KBr pellets. OLYMPUS BTX III X-ray diffraction (XRD) analyser was used to identify the nature of adsorbents. The XRD pattern was obtained by using Cu-kα radiation with λ = 1.54 Å. The surfaces morphology was examined by JEOL JSM-7600F emission scanning electron microscope (SEM) coupled with energy-dispersive X-ray spectroscopy (EDS) in order to provide elemental analysis and quantitative compositional information.

2.3. Preparation of stock solution

A stock solution was prepared by dissolving 1,000 mg of phenol (purity 99.8%, Sigma-Aldrich) in appropriate volume of distilled water to reach 1,000 mg/L then it was stored in a brown coloured glass flask to prevent photo-oxidation. The working solutions were obtained by adequate diluting of stock solution.

2.4. Batch adsorption studies

Factors affecting on the adsorption of phenol were investigated, including pH solution, contact time, adsorbent dosage, initial phenol concentration and temperature. The adsorption parameters were varied in the following ranges: pH 2–12 and pH was adjusted by using 0.1 N NaOH/0.1 N HCl, contact time 5–240 min, adsorbent dosages 0.1–0.6 mg, initial phenol concentration 10–70 mg/L and temperature 25–65°C. All experiments were performed by taking 20 mL phenol solution in 250 mL glass Erlenmeyer flasks and were shaken in orbital at 300 RPM. Each experiment was conducted twice, the average results are presented in this work. The liquid, and solid phases were separated by Grade 1 Whatman Filter Paper (pore size 11 μm). The residual phenol concentration was determined by UV-VIS Spectrophotometer (UV-DR 6000) at the wavelength (λ_{max} = 270 nm). The concentrations of 1, 2, 3, 4, 5, 10, 20, 30, 40 and 50 mg/L of phenol solution were used to draw the calibration graph by plotting them vs. their absorbance. This calibration curve was used to determine the unknown concentrations of phenol. The unknown concentrations of the solutions were determined by using the linear regression obtained by plotting a calibration curve over a range of concentrations.

The adsorption capacity (q_e) (mg/g) for each adsorbent and the percentage removal of phenol (PR) at equilibrium were determined according to the following equations:

$$q_e = \frac{C_0 - C_e}{m} V \tag{1}$$

$$\mathrm{PR}(\%) = \frac{C_0 - C_e}{C_0} \times 100 \tag{2}$$

where C_0 and C_e are initial and equilibrium phenol concentrations (mg/L), respectively. V is the volume of solution (L) and m is the mass of adsorbent (g).

2.5. Equilibrium modelling

Equilibrium data called adsorption isotherms describes how the adsorbates interact with the adsorbents and provide information about their adsorption capacities. Four isotherm models namely Langmuir, Freundlich, Temkin and Dubinin–Radushkevich have been investigated to discuss equilibrium characteristics of phenol adsorption onto NF and ACF.

2.5.1. Langmuir isotherm

The Langmuir isotherm applies to adsorption on homogeneous surfaces with formation of a monomolecular adsorbed layer [22]. The isotherm is represented by the following equation:

$$q_e = \frac{q_m \cdot K_L \cdot C_e}{1 + K_L \cdot C_e} \tag{3}$$

The linear form of the equation can be written as:

$$\frac{C_e}{q_e} = \frac{1}{q_m K_L} + \frac{C_e}{q_m} \tag{4}$$

where q_e is the amount of phenol per unit weight of adsorbent (mg/g), C_e is the equilibrium phenol concentration in the bulk solution (mg/L), q_m is the maximum monolayer adsorption capacity (mg/g), and K_L is the Langmuir constant (L/mg) related to the free energy of adsorption.

2.5.2. Freundlich isotherm

Freundlich isotherm is an empirical model used to describe the adsorption on heterogeneous surfaces with assumption no monolayer capacity [23,24]. This model is represented by the equation below:

$$q_e = K_F \cdot C_e^{1/n} \tag{5}$$

The linear form of this isotherm can be represented by the following equation:

$$\ln q_e = \ln K_F + \left(\frac{1}{n}\right) \ln C_e \tag{6}$$

where K_F is the constant relevant to the relative adsorption capacity of the adsorbent (mg/g) and $1/n$ is the constant relevant to the intensity of the adsorption.

2.5.3. Temkin isotherm

Temkin isotherm is based on the assumption of the heat of adsorption of all the molecules in the layer decreases when the surface of the adsorbent is more covered [24]. Temkin isotherm model is given by the following equation:

$$q_e = \frac{RT}{b_T} \ln\left(K_T C_e\right) \tag{7}$$

The linear form of Temkin isotherm is expressed as:

$$q_e = B \ln K_T + B \ln C_e \tag{8}$$

$$B = \frac{RT}{b_T} \tag{9}$$

where T is absolute temperature (K), R is the universal gas constant (8.314 J/mol·K), K_T and b_T are Temkin isotherm equilibrium binding constant (L/g) and the Temkin constant (J/mol), respectively. B is a constant related to heat of adsorption.

2.5.4. Dubinin–Radushkevich isotherm

Dubinin–Radushkevich isotherm is generally applied to express the adsorption mechanism with a Gaussian energy distribution onto a heterogeneous surface [24]. This isotherm model equation is expressed as:

$$q_e = q_m \exp\left(-\beta \varepsilon^2\right) \tag{10}$$

The linear form of Dubinin–Radushkevich isotherm is:

$$\ln q_e = \ln q_m - \beta \varepsilon^2 \tag{11}$$

where q_e is amount of phenol adsorbed onto adsorbent at equilibrium (mg/g); q_m is theoretical maximum capacity of phenol adsorbed on the adsorbent surface (mg/g); β is Dubinin–Radushkevich isotherm constant ($\mathrm{mol^2/kJ^2}$) and e is the Polanyi potential, corresponding to:

$$\varepsilon = RT \ln\left(1 + \frac{1}{C_e}\right) \tag{12}$$

The constant β represents the adsorption of phenol onto the adsorbent following its transfer from the solution. This activity coefficient is related to the mean free adsorption energy (E) as shown by the following relationship:

$$E = \frac{1}{\sqrt{2\beta}} \tag{13}$$

2.6. Kinetic modelling

The study of adsorption kinetics determines the adsorption rate of phenol and explains the mechanism of its adsorption on the adsorbent surfaces. Among the numerous models available to describe adsorption kinetics,

pseudo-first-order and pseudo-second-order models were applied to fit the experimental data.

2.6.1. Pseudo-first-order model

The pseudo-first-order kinetic model is based on the adsorption capacity. It can be expressed by the following equation:

$$\ln\left(q_e - q_t\right) = \ln q_e - K_1 t \tag{14}$$

where q_e (mg/g) and q_t (mg/g) are the amount of phenol adsorbed at equilibrium and at time t (min), respectively; K_1 (min^{-1}) is the equilibrium rate constant of pseudo-first-order model which can be calculated by plotting $\ln(q_e - q_t)$ vs. t [25].

2.6.2. Pseudo-second-order model

The pseudo-second-order kinetic model is based on the assumption of chemisorption of the phenol on the adsorbent. This model is given by the following equation:

$$\frac{t}{q_t} = \frac{1}{K_2 q_e^2} + \frac{1}{q_e} t \tag{15}$$

where K_2 (g/mg·min) is the rate constant of the pseudo-second-order adsorption which can be calculated by plotting t/q_t vs. t [26].

2.7. Diffusion modelling

In order to understand the diffusion mechanism and mass transfer processes, two mechanism models have been studied:

2.7.1. Liquid film diffusion model

Liquid film diffusion model can be described as:

$$\ln\left(1 - \frac{q_t}{q_e}\right) = -K_{fd} t + C \tag{16}$$

where K_{fd} (min^{-1}) is the rate coefficient for particle-diffusion controlled process corresponding to the particle size of the adsorbent [27].

2.7.2. Intraparticle diffusion model

Intraparticle diffusion model is commonly used to identify the adsorption mechanism for design purpose. It can be represented by the following equation:

$$q_t = K_{id} t^{0,5} + C \tag{17}$$

where K_{id} is the intraparticle diffusion rate constant (mg/g·$min^{0.5}$) and C is a constant related to the thickness of the boundary layer [27,28].

2.8. Adsorption thermodynamics

Thermodynamic behaviour of phenol adsorption onto NF and ACF was revealed by calculating thermodynamic parameters such as standard free energy change ($\Delta G°$), standard enthalpy change ($\Delta H°$) and standard entropy change ($\Delta S°$) using the following equations [29].

$$\Delta G^0 = -RT \ln K^0 \tag{18}$$

$$\ln K^0 = \frac{\Delta S^0}{R} - \frac{\Delta H^0}{RT} \tag{19}$$

where K^0 is the thermodynamic equilibrium constant (L/g), R is the universal gas constant (8.314 J/mol·K) and T is the absolute temperature (K). $\Delta H°$ (kJ/mol) and $\Delta S°$ (kJ/mol·K) values of the adsorption process were calculated from the Van't Hoff equation [Eq. (19)], from the slope and intercept of the plot $\ln K^0$ of vs. $1/T$.

3. Results and discussions

3.1. Characterisation of CN and ACF

3.1.1. Nitrogen sorption

The textural characteristics of the adsorbents obtained by nitrogen adsorption–desorption technique are presented in Table 1. It can be clearly observed that the BET surface area, the total pore volume and the micro pore volume of ACF are significantly greater than the values obtained for NF, which indicate the development of raw material characteristic under activation mode effects [30]. The presence of pores is the responsible factor for big surface area, so low porosity material means low surface area. The pore size of the adsorbents is larger than 2 nm, as shown by the BET method and confirmed by the BJH values. According to the International Union of Pure and Applied Chemistry (IUPAC), the values of average pore diameter indicate that both prepared adsorbents are characterized as mesoporous [31]. Due to their high mesopore content, NF and ACF adsorbents can be excellent adsorbents for organic pollutants of medium molecular size (>2 nm).

3.1.2. Infrared spectroscopy

The IR spectrums of NF and ACF are illustrated in Fig. 1. The number and intensity of peaks in the NF spectrum are higher than in the ACF spectrum. This may be due to the thermal degradation of some intermolecular bonds during the activation process [32]. The peaks at 3,423.83 cm^{-1} indicate the stretching vibrations of O-H bonds in a hydroxyl group of carbohydrate (hemicellulose and cellulose) and lignin of *Phoenix dactylifera* fiber, while the peak at 2,923.57 cm^{-1} is related to the C–H stretching vibration of aliphatic chain in fiber components [33]. For ACF, the first peak has lost its intensity and the second-one has disappeared. These two cases may be caused by the evaporation of moisture and volatile contents [32]. For both samples, the peak that appeared at 1,735.63 cm^{-1} was attributed to C=O stretching vibrations in the acetyl and carboxylic acid groups [34]. Whereas the peak at 1,616.06 cm^{-1} belong to aromatic C=C bond. After the last-mentioned point, the ACF showed no peak, which confirms the hypothesis that many bonds are broken due to activation. Moreover, low

Table 1
Textural characteristics of NF and ACF

Sample	S_{BET} (m^2/g)	S_{ext} (m^2/g)	S_{mic} (m^2/g)	V_{tot} (cm^3/g)	V_{mic} (cm^3/g)	D_{BET} (nm)	D_{BJH} (nm)
NF	1.108	0.0524	1.0554	0.000576	0.000513	2.0815	2.5784
ACF	269.543	69.057	200.486	0.146	0.0985	2.163	2.962

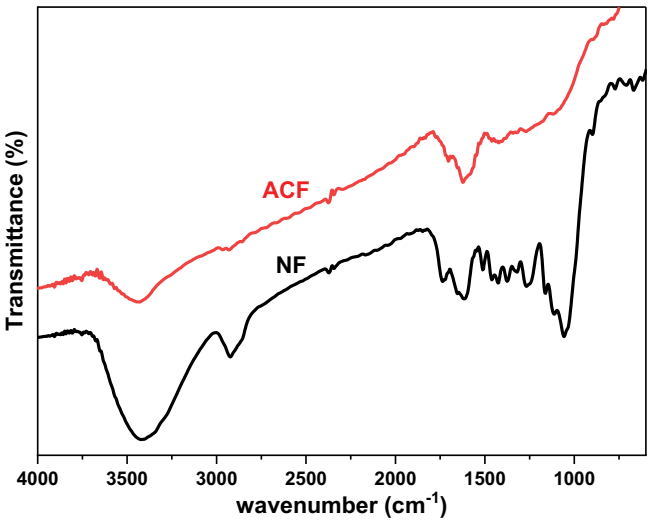

Fig. 1. FTIR spectra of natural fiber (NF) and activated carbon fiber (ACF).

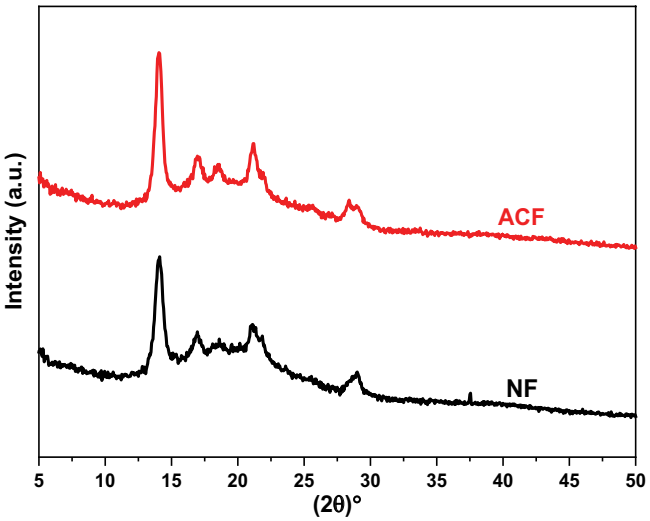

Fig. 2. XRD diffractograms of natural fiber (NF) and activated carbon fiber (ACF).

intensity bands at 1,511.93 and 1,427.07 cm^{-1} were indexed to the stretching vibration of aromatic C–H group and carboxylate groups [33]. The peak due to alcohol group of cellulose (δ OH deformation) is located at 1,376.65 cm^{-1} [35]. The existence of peaks at 1,276.65 and 1,060.66 cm^{-1} represents –C–O–C– and C–H stretching of cellulose and lignin, respectively [33].

3.1.3. X-ray diffraction

The X-ray diffraction patterns present in Fig. 2 shows the amorphous structure of raw NF and ACF that could be seen as broad diffraction at 16.05° and 26.1°. Furthermore, the sharp peaks at 2θ values (14.150, 17.20, 18.80, 21.250 and 29.150) shows the presence of some cellulose crystalline region [36,37]. The amorphous structure of the precursor was attributed to the high amount of hemicellulose and lignin content. It can be seen that the amorphous region of raw material was reduced after its transformation into activated carbon. The small decrease in the amorphous region of raw material is due to the exposure of hemicellulose and lignin to high temperature during carbonization [38,39].

3.1.4. Scanning electron microscopy

Scanning electron microscopy (SEM) images of NF and ACF are shown in Fig. 3. The micrographs show that both samples have an irregular shape. The SEM image of NF shows more white spots with a mixed surface from smooth to coarse. ACF surface has fewer white spots, signifying a rough and heterogeneous surface with many pores created. These observations could contribute to the high surface area and pore volume of activated carbon [40].

3.1.5. Elemental analysis

The elemental composition of NF and ACF was determined by the EDS analysis. The results presented in Fig. 3 show that NF contains 66.18% of carbon and 33.09% of oxygen, while ACF contains 78.71% of carbon and 20.64% of oxygen. This means an increase of 12.53% in the carbon content and a decrease in oxygen content by 12.45% after chemical activation and carbonization. A considerable amount of carbon provided an active surface for phenol fixation on the adsorbent surface [40]. The Si peak show in both samples may have originated from the diode probe of the apparatus. For activated carbon, the absence of phosphorus indicates the effectiveness of washing after its preparation, but the presence of zirconium indicates its subsequent contamination.

3.2. Effect of adsorption parameters

3.2.1. Effect of pH

The solution pH is a critical parameter that influences the adsorption process due to its effect on the adsorbent surface charge and the ionisation degree of the adsorbate [41]. The experiment was performed by following conditions (pH = 2–12, 0.1 g of sorbents, T = 25°C and t = 2 h). As presented in Fig. 4, low-rate adsorption values were found

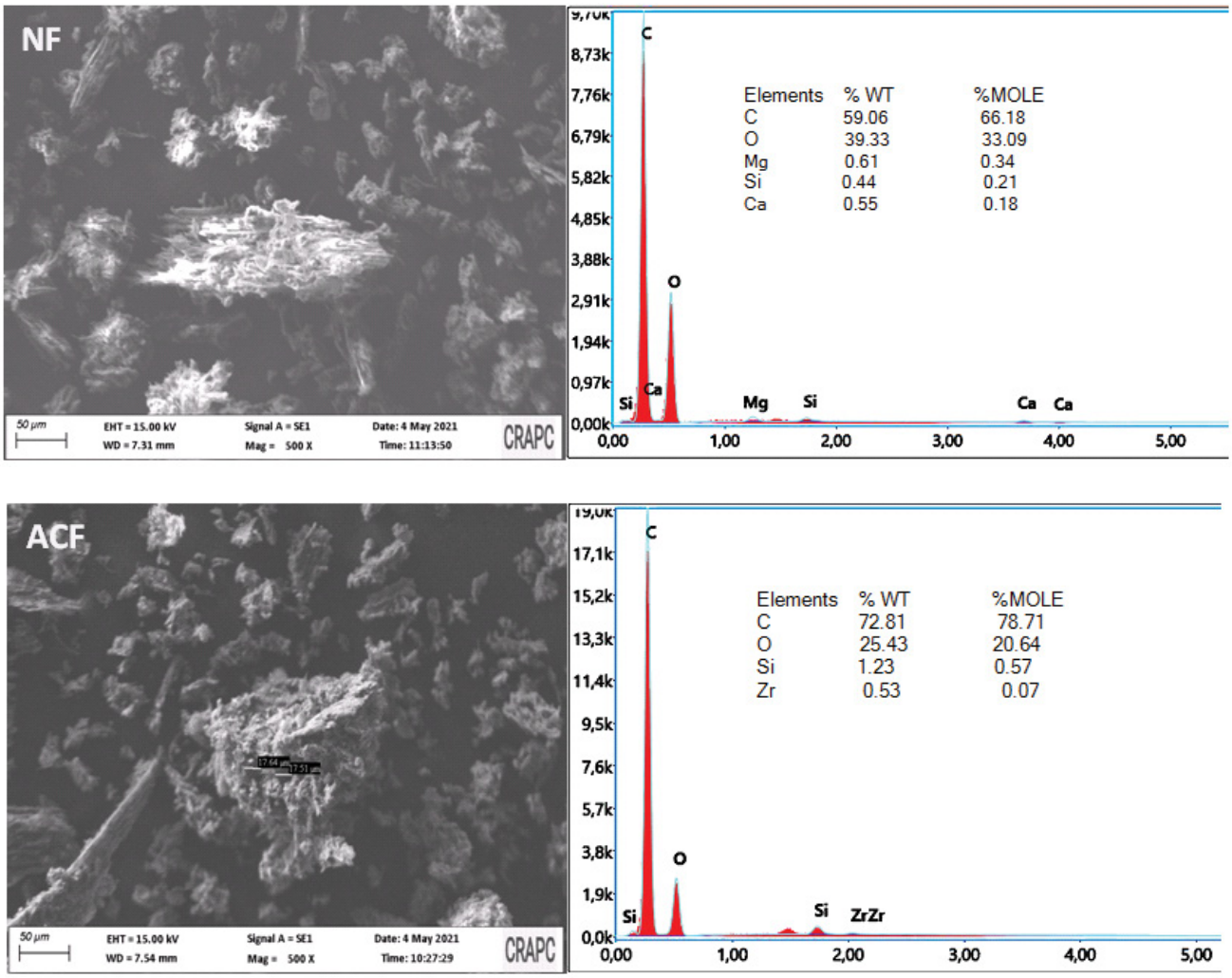

Fig. 3. SEM-EDS analysis of natural fiber (NF) and activated carbon fiber (ACF).

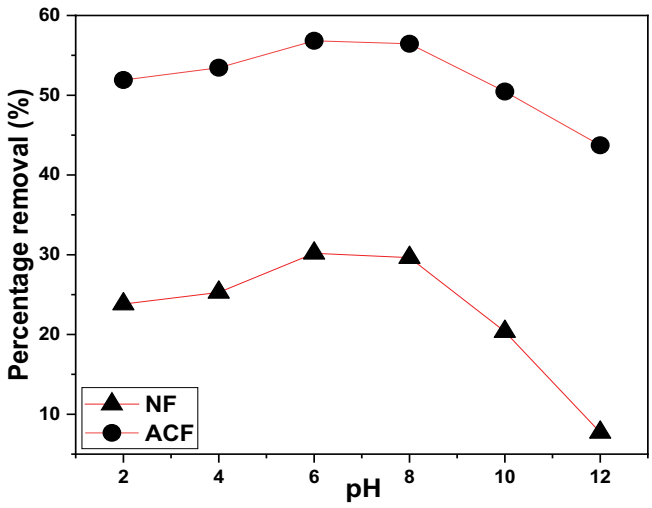

Fig. 4. Effect of pH on phenol adsorption onto natural fiber (NF) and activated carbon fiber (ACF) (adsorbent dosage = 0.1 g; temperature = 25°C; contact time = 120 min; initial phenol concentration = 50 mg/L).

in pH = 2–6 due to protonation of adsorbents surface which led to donor–acceptor interactions between the aromatic rings of the phenol [42]. The optimum adsorption capacities of phenol take place in the pH region 6–8 and this is caused by electrostatic interaction between the positive ions on the surface and phenolate ions [43]. However, the percentage removals were decreased with the pH greater than 8 due to the ionization of phenol and the electrostatic repulsion force between negative adsorbents sites and phenolate ions ($C_6H_5O^-$) which are more soluble in the aqueous solution, and form strong adsorbate–water bonds [44]. As the value of pH at 6 gave the maximum percentage phenol removals (30.18% for NF and 56.81% for ACF), it was selected for further studies. Similar result has been reported for adsorption of phenol on modified activated carbon [45].

3.2.2. *Effect of contact time*

Fig. 5 presents the effect of contact time on phenol adsorption. According to the results, a high percentage of phenol was removed at the first 15 min due to the abundance of available vacant surface sites [3,46]. Thereafter,

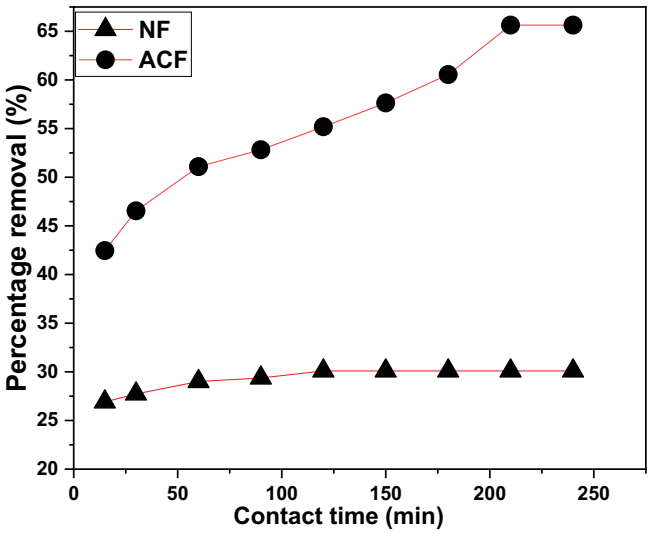

Fig. 5. Effect of contact time on phenol adsorption onto natural fiber (NF) and activated carbon fiber (ACF) (adsorbent dosage = 0.1 g; temperature = 25°C; pH = 6; initial phenol concentration = 50 mg/L).

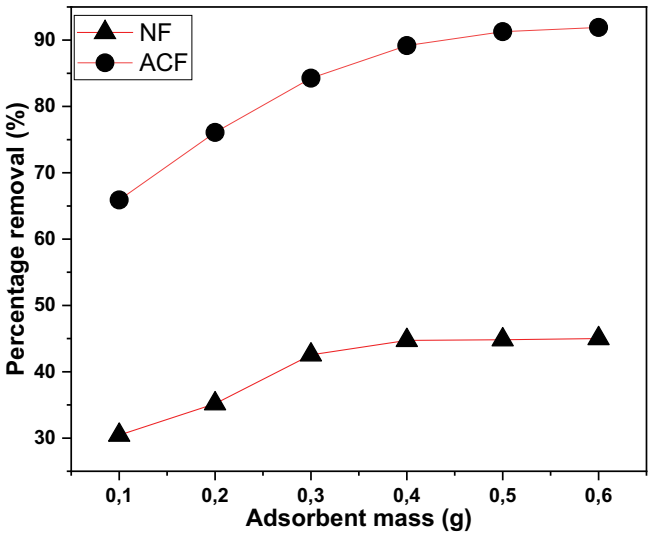

Fig. 6. Effect of adsorbents mass on phenol adsorption onto natural fiber (NF) and activated carbon fiber (ACF) (contact time = 120 min for NF and 210 min for ACF; temperature = 25°C; pH = 6; initial phenol concentration = 50 mg/L).

the removal becomes slower until the equilibrium points, at 120 and 210 min on NF and ACF, respectively. This phenomenon can be explained by the fact that the remaining empty sites are difficult to occupy by the phenol molecules due to the repulsive forces between the phenol on the solid and solution phase [3]. It's natural that ACF takes longer time to reach to equilibrium because it contains more adsorption sites than the other.

3.2.3. Effect of adsorbent mass

As shown in Fig. 6, the percentage of phenol removed increases with the adsorbent mass, with maximum phenol removal of 45% and 91.9% for NF and ACF, respectively. This increase is due to the availability of a greater number of sorption sites [47]. The optimum mass for NF and ACF are respectively 0.4 and 0.5 g, since there is no significant increase in phenol removal rate above these values.

3.2.4. Effect of initial concentrations

Fig. 7 reveals the effect of initial concentration on the phenol removal onto both adsorbents. The results show that the adsorption capacity increases with the initial phenol concentration due to a weakness of the solid resistance to phenol mass transfer from the liquid [48].

In the case of NF, increasing the initial phenol concentration leads to a decrease in the percentage of its removal. At high concentrations, a large part of the phenol remains in solution due to limited number of active sites.

For ACF, the percentage of phenol removal increases with increasing initial concentrations. This is because the active sites on the adsorbent surface were not fully occupied by phenol [49]. The same phenomenon was observed in the adsorption of phenol from aqueous solution on fly ash from a thermal power plant [50]. It can be concluded that the percentage phenol removal is highly dependent on the initial phenol concentration.

3.2.5. Effect of temperatures

The graphs in Fig. 8 show a decrease in the percentage phenol removal with increasing temperature for both adsorbents. This shows that the lowest removal rates were recorded at the highest temperatures. This result is mainly due to the weakening of the sorption forces between the active sites on the adsorbents and the adsorbed species, in one side, and between adjacent phenol molecules on the adsorbed phase, in the other side. In addition to the reasons mentioned above, increasing temperature enhances the desorption step in the sorption mechanism, indicating that the process is exothermic [51,52]. The same behaviour was found by different researchers for adsorption of phenol on modified activated carbon [45], *Luffa cylindrica* fibers [51] and palmkernel fibre [52], respectively.

3.3. Adsorption isotherm study

The results of the equilibrium isotherm modelling are presented in Fig. 9 and Table 2. According to the results, the adsorption of phenol on NF and ACF is well described by the Freundlich model with the highest correlation coefficients (R^2 = 0.9848 and R^2 = 0.9873). The best fit of this model to the experimental data suggests the presence of heterogeneous adsorption sites on the adsorbent surface [53]. Concerning NF, the Temkin isotherm also shows a good correlation, with an R^2 value of 0.9827 indicating mixed adsorption behaviour on the NF surface. The suitability of Freundlich model for phenol absorption has been also reported by Mojoudi et al. [54] using high microporous activated carbons prepared from oily sludge, and Lütke et al. [53] from activated carbon prepared from black wattle bark waste.

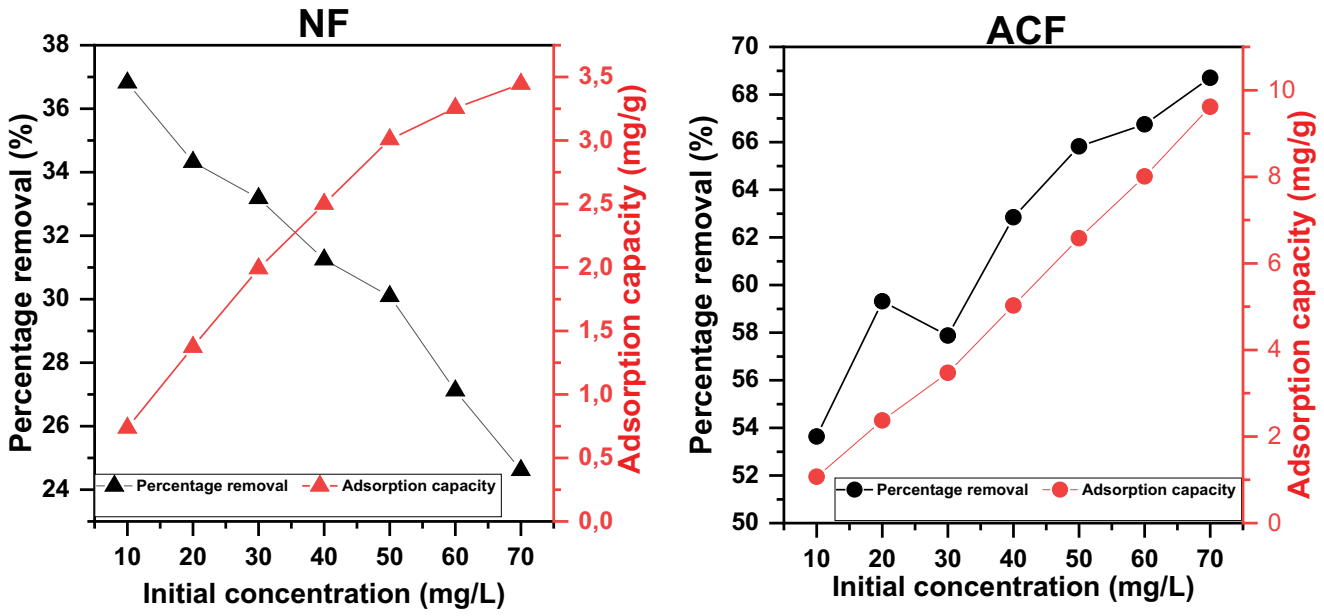

Fig. 7. Effect of initial phenol concentrations on the adsorption process by natural fiber (NF) and activated carbon fiber (ACF) (adsorbent dosage = 0.1 g; contact time = 120 min for NF and 210 min for ACF, temperature = 25°C; pH = 6).

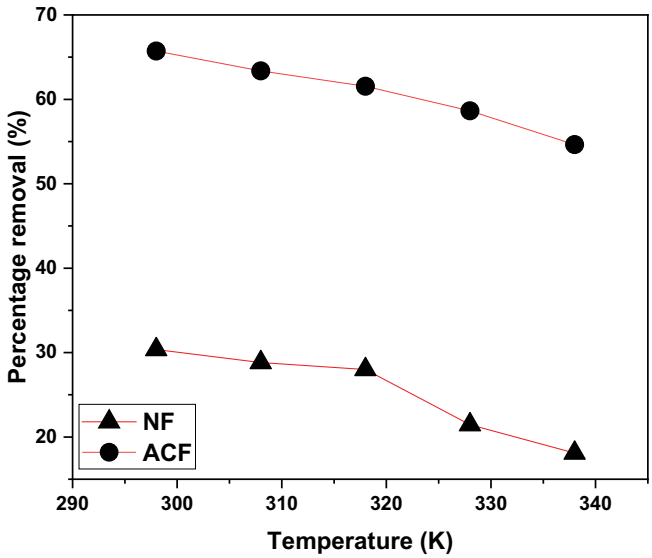

Fig. 8. Effect of temperatures onto phenol adsorption by natural fiber (NF) and activated fiber carbon (ACF) (adsorbent dosage = 0.1 g; contact time = 120 min for NF and 210 min for ACF; pH = 6; initial phenol concentration = 50 mg/L).

Moreover, other important and useful information could be obtained from Table 2, including the nature of the adsorption (exothermic or endothermic), the theoretical maximum adsorption capacity and whether the adsorption of phenol was favourable or unfavourable.

A value of $1/n$ less than 1 suggests a favorable adsorption for NF, whereas for ACF, a cooperative adsorption process occurs when $1/n > 1$ [55]. The positive sign of b_T from Temkin model for both studied states, indicating that the adsorption reaction is exothermic [56]. While, the values of b_T refer to a physical adsorption process. The mean free adsorption energy (E) for phenol removal process on NF and ACF was 0.223 and 0.235 kJ/mol, respectively. These values less than 8 kJ/mol emphasize the physical nature of phenol removal [57].

Table 3 shows a comparison of the results obtained in this study with the phenol maximum adsorption capacities onto several adsorbents.

3.4. Kinetic study

The kinetics of phenol uptake onto NF and ACF were studied using two common models. The graphical presentation of the kinetic models is presented in Fig. 10, while the calculated parameters are collected in Table 4. It is obvious from results that the pseudo-second-order model fits the experimental data better than pseudo-first-order model because of the R^2 values are close to unity and the calculated $q_{e,cal}$ values are close to the experimental $q_{e,exp}$ values for NF and ACF. Thus, the obtained results illustrate that chemical sorption is effective in phenol adsorption onto NF and ACF [63]. Furthermore, the sorption capacity is proportional to the number of active sites occupied on the sorbents [64,26]. Similar results were observed in the adsorption of phenol on Na bentonite [28] and high microporous activated carbons prepared from oily sludge [54].

3.5. Diffusion study

Fig. 11 shows the plots of the liquid film diffusion (LFD) and intraparticle diffusion (IPD) models. As it can be seen from Fig. 11a, the plots reveal two distinct linear phases, indicating that the adsorption of phenol occurred in a two-step intraparticle diffusion process. The first linear phase may be due to the external mass transfer of phenol to the sorbent particles. The second linear phase represents the

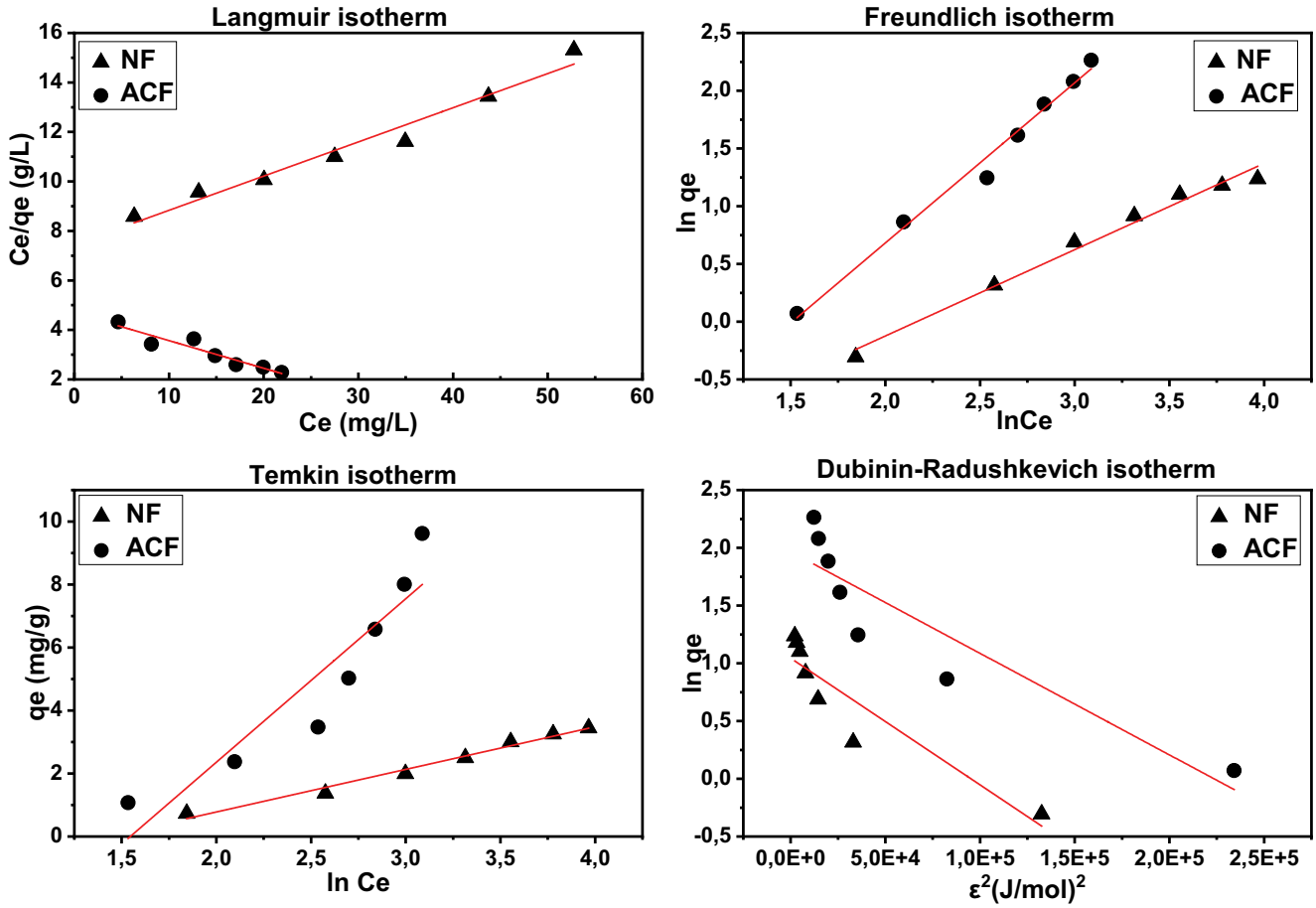

Fig. 9. Adsorption isotherms of phenol onto natural fiber (NF) and activated carbon fiber (ACF).

Table 2
Isotherm parameters for phenol adsorption onto NF and ACF

Isotherm	Parameters	NF	ACF
Langmuir	q_m (mg/g)	7.236	–8.952
	K_L (L/mg)	0.0185	–0.0238
	R^2	0.9689	0.9012
Freundlich	K_F (L/g)	0.198	0.1234
	n	1.338	0.721
	R^2	0.9848	0.9873
Temkin	K_T (L/g)	0.241	0.213
	b_T (kJ/mol)	0.183	0.477
	B	1.3522	5.19
	R^2	0.9827	0.8586
Isotherm (Dubinin–Radushkevich)	q_m (mg/g)	2.84	7.141
	β (mol²/J⁻²)	10^{-5}	9×10^{-6}
	E (kJ/mol)	0.223	0.235
	R^2	0.855	0.8366

Table 3
Comparison of maximum adsorption capacities of phenol by various adsorbents

Adsorbent	q_{max} (mg/g)	Reference
NF	3.45	This study
ACF	9.62	This study
SDS-alumina	6.64	[58]
Carbon-encapsulated iron nanoparticles (CEINs)	5.1	[59]
Graphene oxide (GO)	3.96	[60]
AC-Al_2O_3	3.55	[61]
AC-Fe_2O_3	3.29	[61]
AC-TiO_2	3.15	[61]
AC purchased	1.51	[61]
Activated coal	1.48	[62]

slower pore volume diffusion at the equilibrium phase of the reaction [65].

In Table 5, it is important to note that the values of the thickness C calculated from the IPD model are greater than zero, suggesting that the boundary layer thickness participated in the adsorption process [27,66]. Neither the (IPD) nor the (LFD) plot passes through the origin (Fig. 11), indicating that the adsorption process is not solely controlled by intraparticle diffusion or film diffusion [67]. The R^2 values confirmed that the effect of intraparticle diffusion on the

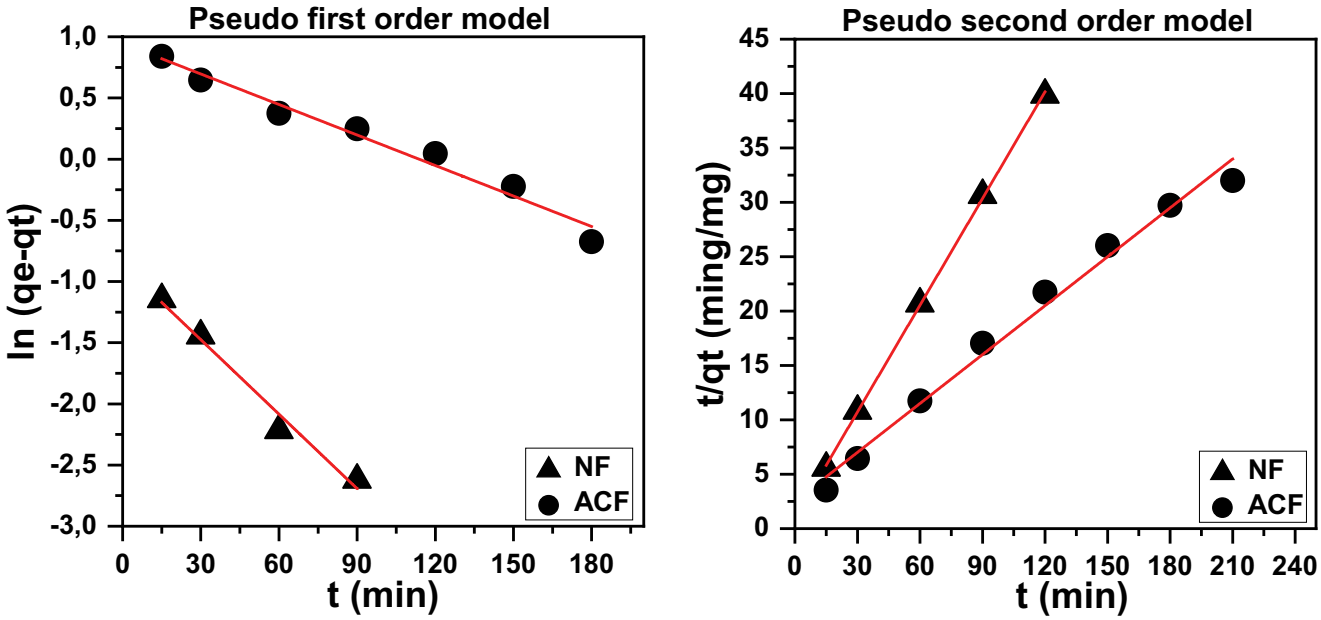

Fig. 10. Kinetic models for phenol adsorption onto NF and ACF.

Table 4
Kinetic parameters of phenol removal by NF and ACF

Samples	Experimental	Pseudo-first-order			Pseudo-second-order		
	$q_{e,exp}$ (mg/g)	$q_{e,cal}$ (mg/g)	K_1 (min^{-1})	R^2	$q_{e,cal}$ (mg/g)	K_2 (g/mg·min)	R^2
NF	3.009	0.420	0.0203	0.9826	3.057	0.117	0.9997
ACF	6.564	2.574	0.0083	0.9742	6.671	0.0089	0.9879

Table 5
Diffusion parameters of phenol adsorption onto NF and ACF

Samples	Intraparticle diffusion			Liquid film diffusion		
	K_{id} (mg/g·min$^{0.5}$)	C_1	R^2	K_{fd} (min^{-1})	C	R^2
NF	0.0245	2.6665	0.8194	0.0203	–1.9683	0.9826
ACF	0.1909	3.5391	0.9786	0.0083	0.9362	0.9742

adsorption process for ACF was more important than for NF. Through the aforementioned, another diffusion model may be involved in the determination of the rate control step.

3.6. Thermodynamics analysis

The thermodynamic parameters reflect the spontaneous nature and the feasibility of a sorption process. $\Delta H°$ and $\Delta S°$ were calculated from the slope and intercept of the plot $\ln K^0$ vs. $1/T$ (Fig. 12) and $\Delta G°$ values were calculated from Eq. (18). These parameters are reported in Table 6. The positive values $\Delta G°$ values confirmed that the adsorption of phenol onto NF and ACF was not spontaneous [68]. Moreover, increasing the temperature from 25°C to 65°C led to an increase in $\Delta G°$ values, thus the adsorption was not favourable at high temperatures for both adsorbents. This was proved by negative values of $\Delta H°$, which confirmed the exothermic nature of the adsorption onto both sorbents, and supported by the decrease in phenol adsorption values, with increasing temperature. The negative $\Delta S°$ values show a decrease in the randomness at the adsorbent–phenol interface during adsorption [69].

4. Conclusion

This work reported on the utilization of natural *Phoenix dactylifera* fiber (NF) and *Phoenix dactylifera* fiber chemically activated with H_3PO_4 (ACF) for phenol removal from wastewater. The characterization of adsorbents confirms that the activation mode resulted in a significant improvement in textural properties without damaging the crystalline structure of NF.

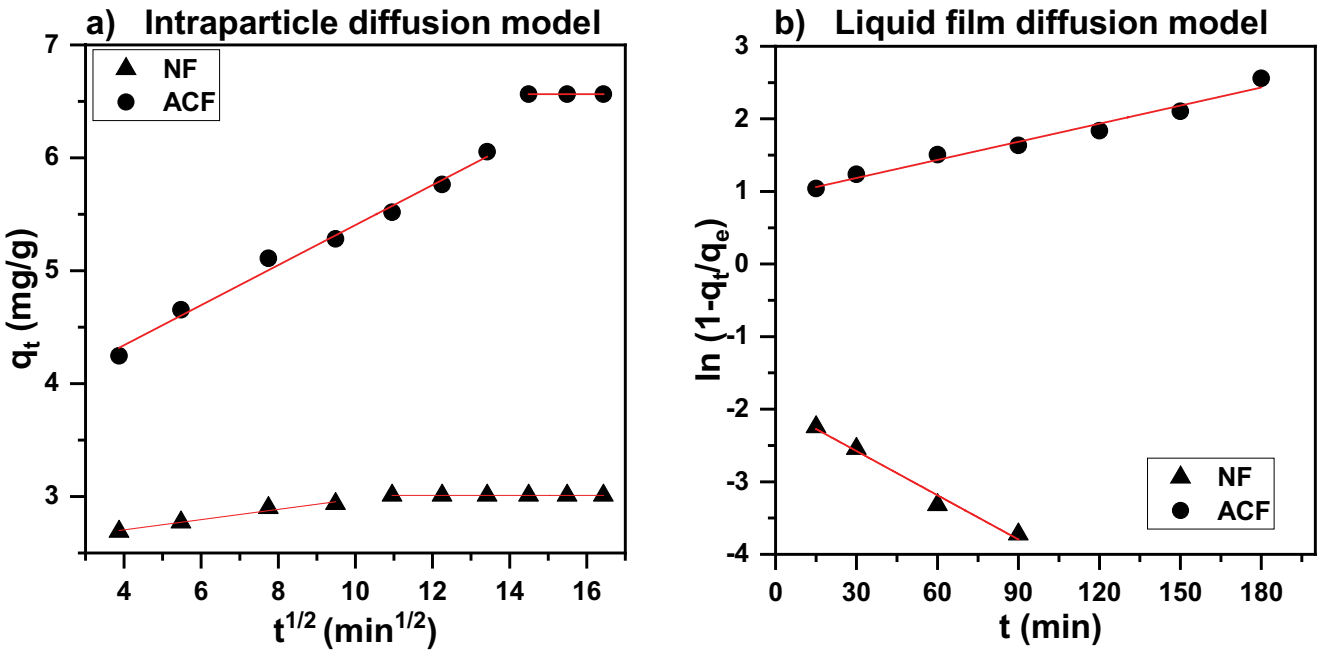

Fig. 11. Diffusion models of phenol adsorption onto NF and ACF.

Table 6
Thermodynamic parameters of phenol adsorption onto NF and ACF

Samples	NF			ACF		
Temperatures (K)	$\Delta G°$ (kJ/mol)	$\Delta H°$ (kJ/mol)	$\Delta S°$ (kJ/mol·K)	$\Delta G°$ (kJ/mol)	$\Delta H°$ (kJ/mol)	$\Delta S°$ (kJ/mol·K)
298	6.044			2.374		
308	6.437			2.718		
318	6.752	–14.519	–0.068	3.012	–9.406	–0.039
328	7.928			3.437		
338	8.767			4.000		

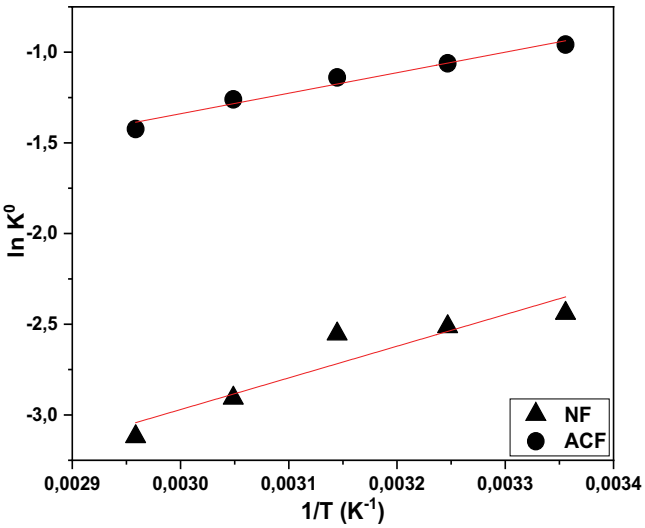

Fig. 12. Variation of lnK^0 as a function of 1/T for phenol adsorption using NF and ACF.

Phenol removal efficiency was significantly affected by several parameters such as the pH solution, contact time, initial phenol concentration, adsorbent dosage and temperature. Using phenol concentration of 50 mg/L, 300 rpm agitation speed, pH = 6 and temperature of 25°C, the optimum removal of phenol was attained to 44.7% at 120 min and dose of 0.4 mg/L for NF, while it was achieved to 91.3% at 210 min and dose of 0.5 mg/L for ACF. Additionally, the fastest adsorption rates were within the first 15 min, followed by equilibrium.

This study showed an unusual phenomenon for ACF, which was represented by an increase in the percentage of phenol removal when the concentration of phenol increase. In contrast to NF, the increase in the concentration of phenol leads to a decrease in the percentage of phenol removal, which concludes that NF is suitable for low concentrations, while ACF is suitable for high concentrations.

Based on experimental results, the maximum adsorption capacities were 3.45 and 9.62 mg/g for NF and ACF, respectively. The value of the maximum absorbent capacity of raw *Phoenix dactylifera* fiber is satisfactory compared

to some of the activated sorbents cited in literature. The isotherm and kinetic data were well described by the Freundlich and pseudo-second-order models as indicated by correlation coefficients. Moreover, the thermodynamic parameters obtained indicate that the adsorption process onto NF and ACF is exothermic and non-spontaneous. It can be concluded that the prepared sorbents had acceptable phenol adsorption performance, low dose requirements, simplicity as well as low cost.

Acknowledgments

The authors are thankful to the staff of Sahara Geology Laboratory and Scientific and Technical Research Centre for Physical and Chemical analysis, for their valuable cooperation in the achievement of experimental tests.

Disclosure statement

The authors reported no potential conflict of interest.

References

[1] K. Pirzadeh, A.A. Ghoreyshi, Phenol removal from aqueous phase by adsorption on activated carbon prepared from paper mill sludge, Desal. Water Treat., 52 (2014) 6505–6518.
[2] K. Mainali, Phenolic compounds contaminants in water: a glance, Curr. Trends. Civ. Struct. Eng., 4 (2020) 1–3.
[3] S. Rahdar, M. Ahamadabadi, R. Khaksefidi, M. Saeidi, M.R. Narooie, A. Salimi, H. Biglari, M.M. Baneshi, Evaluation of phenol removal from aqueous solution by banana leaf ash, J. Global Pharm. Technol., 9 (2017) 20–28.
[4] S. Golbaz, A.J. Jafari, M. Rafiee, R.R. Kalantary, Separate and simultaneous removal of phenol, chromium, and cyanide from aqueous solution by coagulation/precipitation: mechanisms and theory, Chem. Eng. J., 253 Complete (2014) 251–257.
[5] L.H. Gracioso, P.B. Vieira, M.P.G. Baltazar, I.R. Avanzi, B. Karolski, C.A.O. Nascimento, E.A. Perpetuo, Removal of phenolic compounds from raw industrial wastewater by *Achromobacter* sp. isolated from a hydrocarbon-contaminated area, Water Environ. J., 33 (2018) 1–11.
[6] F. Zhang, K. Wu, H. Zhou, Y. Hu, P. Sergei, H. Wu, C. Wei, Ozonation of aqueous phenol catalyzed by biochar produced from sludge obtained in the treatment of coking wastewater, J. Environ. Manage., 224 (2018) 376–386.
[7] J. Fan, H. Wu, R. Liu, L. Meng, Y. Sun, Review on the treatment of organic wastewater by discharge plasma combined with oxidants and catalysts, Environ. Sci. Pollut. Res., 28 (2021) 2522–2548.
[8] G. Fadillah, T.A. Saleh, S. Wahyuningsih, Enhanced electrochemical degradation of 4-nitrophenol molecules using novel Ti/TiO_2-NiO electrodes, J. Mol. Liq., 289 (2019) 1–20.
[9] M.A. Farajzadeh, M.R. Fallahi, Study of phenolic compounds removal from aqueous solution by polymeric sorbent, J. Chin. Chem. Soc., 52 (2005) 295–301.
[10] M. Ahmaruzzaman, Adsorption of phenolic compounds on low-cost adsorbents: a review, Adv. Colloid Interface Sci., 143 (2008) 48–67.
[11] A. Ahmadi, R. Foroutan, H. Esmaeili, S.J. Peighambardoust, S. Hemmati, B. Ramavandi, Montmorillonite clay/starch/$CoFe_2O_4$ nanocomposite as a superior functional material for uptake of cationic dye molecules from water and wastewater, Mater. Chem. Phys., 284 (2022) 126088, doi: 10.1016/j.matchemphys.2022.126088.
[12] M. Dudziak, S. Werle, Studies on the adsorption of phenol on dried sewage sludge and solid gasification by-products, Desal. Water Treat., 57 (2014) 1067–1074.
[13] R. Foroutan, S.J. Peighambardoust, M. Amarzadeh, A.K. Korri, N.S. Peighambardoust, A. Ahmad, B. Ramavandi, Nickel ions abatement from aqueous solutions and shipbuilding industry wastewater using ZIF-8-chicken beak hydroxyapatite, J. Mol. Liq., 356 (2022) 119003, doi: 10.1016/j.molliq.2022.119003.
[14] T.A. Oyehan, F.A. Olabemiwo, B.S. Tawabini, T.A. Saleh, The capacity of mesoporous fly ash grafted with ultrathin film of polydiallyldimethyl ammonium for enhanced removal of phenol from aqueous solutions, J. Cleaner Prod., 263 (2020) 1–10.
[15] M.D. Víctor-Ortega, J.M. Ochando-Pulido, A. Martínez Férez, Equilibrium studies on phenol removal from industrial wastewater through polymeric resins, Sep. Purif. Technol., 47 (2016) 253–258.
[16] T. Jamnongkan, N. Intaramongkol, N. Kanjanaphong, K. Ponjaroen, W. Sriwiset, R. Mongkholrattanasit, P. Wongwachirakorn, K.-Y.A. Lin, C.-F. Huang, Study of the enhancements of porous structures of activated carbons produced from durian husk wastes, Sustainability, 14 (2022) 5896, doi: 10.3390/su14105896.
[17] M. Doloksaribua, B. Prihandokob, K. Triyanac, Harsojod, Preparation and characterization of activated carbon based on coconut shell for supercapacitor, Int. J. Sci.: Basic Appl. Res., 35 (2017) 430–437.
[18] M. Danish, T. Ahmad, R. Hashim, N. Said, M.N. Akhtar, J. Mohamad-Saleh, O. Sulaiman, Comparison of surface properties of wood biomass activated carbons and their application against rhodamine B and methylene blue dye, Surf. Interfaces, 11 (2018) 1–13.
[19] F.J. Tuli, A. Hossain, A.K.M. Fazle Kibria, A.R.M. Tareq, S.M.M.A. Mamun, A.K.M. Atique Ullah, Removal of methylene blue from water by low-cost activated carbon prepared from tea waste: a study of adsorption isotherm and kinetics, Environ. Nanotechnol. Monit. Manage., 14 (2020) 1–8.
[20] P.T. Dhorabe, D.H. Lataye, R.S. Ingole, Removal of 4-nitrophenol from aqueous solution by adsorption onto activated carbon prepared from acacia glauca sawdust, Water Sci. Technol., 73 (2015) 955–966.
[21] A. Kumar, H.M. Jena, Removal of methylene blue and phenol onto prepared activated carbon from fox nutshell by chemical activation in batch and fixed-bed column, J. Cleaner Prod., 137 (2016) 1246–1259.
[22] I. Langmuir, The Adsorption of gases on plane surfaces of glass, mica and platinum, J. Am. Chem. Soc., 40 (1918) 1361–1403.
[23] C.R. Girish, Various isotherm models for multicomponent adsorption: a review, Int. J. Civ. Eng., 8 (2017) 80–86.
[24] A.A. Inyinbor, F.A. Adekola, G.A. Olatunji, Kinetics, isotherms and thermodynamic modeling of liquid phase adsorption of rhodamine b dye onto *Raphia hookerie* fruit epicarp, Water Resour. Ind., 15 (2016) 14–27.
[25] A.A. Ahmad, B.H. Hameed, N. Aziz, Adsorption of direct dye on palm ash: kinetic and equilibrium modeling, J. Hazard. Mater., 141 (2007) 70–76.
[26] Y.S. Ho, G. McKay, Pseudo-second-order model for sorption processes, Process Biochem., 34 (1999) 451–465.
[27] J.O. Ojediran, A.O. Dada, S.O. Aniyi, R. David, A.D. Adewumi, Mechanism and isotherm modeling of effective adsorption of malachite green as endocrine disruptive dye using acid functionalized maize cob (AFMC), Sci. Rep., 11 (2021) 1–15.
[28] H. Asnaoui, Y. Dehmani, M. Khalis, E. Hachem, Adsorption of phenol from aqueous solutions by Na–bentonite: kinetic, equilibrium and thermodynamic studies, J. Environ. Anal. Chem., 102 (2022) 3043–3057.
[29] R.I. Yousef, B. El-Eswed, A.H. Al-Muhtaseb, Adsorption characteristics of natural zeolites as solid adsorbents for phenol removal from aqueous solutions: kinetics, mechanism, and thermodynamics studies, Chem. Eng. J., 171 (2011) 1143–1149.
[30] Y. Önal, C. Akmil-Başar, Ç. Sarıcı-Özdemir, S. Erdoğan, Textural development of sugar beet bagasse activated with $ZnCl_2$, J. Hazard. Mater., 142 (2007) 138–143.
[31] A.J. Jafari, A. Alahabadi, M.H. Saghi, Z. Rezai, A. Rastegar, M.S. Zamani, P. Singh, A. Hosseini-Bandegharaei, Adsorptive removal of phenol from aqueous solutions using chemically activated rice husk ash: equilibrium, kinetic, and thermodynamic studies, Desal. Water. Treat., 158 (2019) 233–244.

[32] A. Melliti, V. Srivastava, J. Kheriji, M. Sillanpää, B. Hamrouni, Date palm fiber as a novel precursor for porous activated carbon: optimization, characterization and its application as tylosin antibiotic scavenger from aqueous solution, Surf. Interfaces, 24 (2021) 1–12.
[33] S. Raghavendra, G.N. Lokesh, Evaluation of mechanical properties in date palm fronds polymer composites, AIP Conf. Proc., 2057 (2019) 1–5.
[34] T.A. Saleh, A.M. Elsharif, S. Asiri, A.I. Mohammed, H. Dafalla, Synthesis of carbon nanotubes grafted with copolymer of acrylic acid and acrylamide for phenol removal, Environ. Nanotechnol. Monit. Manage., 14 (2020) 1–24.
[35] I. Derrouiche, I. Ben Marzoug, F. Sakli, S. Roudesli, Study of extraction and characterization of ultimate date palm fibers, Adv. Mater., 4 (2015) 7–14.
[36] O.S. Samuel, A.M, Adefusika, In: A.R. Pascual, M.E. Eugenio Martín, Cellulose, IntechOpen, 2019, pp. 1–16 (Online).
[37] J. Jain, S. Jain, S. Sinha, Characterization and thermal kinetic analysis of pineapple leaf fibers and their reinforcement in epoxy, J. Elastomers. Plast., 51 (2018) 1–20.
[38] A.O. Basheer, M.M. Hanafiah, M. Abdulhakim Alsaadi, Y. Al-Douri, M.A. Malek, M. Mohammed Aljumaily, S. Saadi Fiyadh, Synthesis and characterization of natural extracted precursor date palm fibre-based activated carbon for aluminum removal by RSM optimization, Processes, 7(2019) 1–20.
[39] M.I. Nasir, M.Z. Hossain, P.A. Charpentier, Synthesis and characterization of date palm fiber-based bio-char and activated carbon and its utilization for environmental remediation, J. Pet. Res. Stud., 8 (2018) 209–222.
[40] A. Machrouhi, H. Alilou, M. Farnane, S. El Hamidi, M. Sadiq, M. Abdennouri, H. Tounsadi, N. Barka, Statistical optimization of activated carbon from *Thapsia transtagana* stems and dyes removal efficiency using central composite design, J. Sci.: Adv. Mater. Devices, 4 (2019) 544–553.
[41] Z. Aksu, E. Kabasakal, Batch adsorption of 2,4-dichlorophenoxy-acetic acid (2,4-D) from aqueous solution by granular activated carbon, Sep. Purif. Technol., 35 (2003) 223–240.
[42] M.A. Khan, A. Ahmad, Kinetics and thermodynamic studies of phenol adsorption on nanocomposite, Desal. Water Treat., 57 (2016) 11255–11265.
[43] A.M. Channa, S. Baytak, S.Q. Memon, M.Y. Talpur, Equilibrium, kinetic and thermodynamic studies of removal of phenol from aqueous solution using surface engineered chemistry, Heliyon, 5 (2019) 1–7.
[44] B. Xie, J. Qin, S. Wang, X. Li, H. Sun, W. Chen, Adsorption of phenol on commercial activated carbons: modelling and interpretation, Int. J Environ. Res. Public Health, 17 (2020) 1–13.
[45] J.Q. Lin, S.E. Yang, J.M. Duan, J.J. Wu, L.Y. Jin, J.M. Lin, Q.L. Deng, M. Jawaid, E.-R. Kenawy, The adsorption mechanism of modified activated carbon on phenol, MATEC Web Conf., 67 (2016) 1–12.
[46] H. Panda, N. Tiadi, M. Mohanty, C.R. Mohanty, Studies on adsorption behavior of an industrial waste for removal of chromium from aqueous solution, S. Afr. J. Chem. Eng., 23 (2017) 132–138.
[47] M.T. Uddin, M.S. Islam, M.A. Islam, M.Z. Abedin, Uptake of phenol from aqueous solution by burned water hyacinth, Pol. J. Chem. Technol., 10 (2008) 43–49.
[48] R.S. Ingole, D.H. Lataye, P.T. Dhorabe, Adsorption of phenol onto banana peels activated carbon, KSCE J. Civ. Eng., 21 (2016) 100–110.
[49] A.S. Muhammad, M.A, Abdurrahman, Adsorption of methylene blue onto modified agricultural waste, Mor. J. Chem., 8 (2020) 412–427.
[50] R. Sharan, G. Singh, S.K. Gupta, Adsorption of phenol from aqueous solution onto fly ash from a thermal power plant, Adsorpt. Sci. Technol., 27 (2009) 267–279.
[51] O. Abdelwahab, N.K. Amin, Adsorption of phenol from aqueous solutions by *Luffa cylindrica* fibers: kinetics, isotherm and thermodynamic studies, Egypt. J. Aquat. Res., 39 (2013) 215–223.
[52] A.E. Ofomaja, Y.S. Ho, Equilibrium sorption of anionic dye from aqueous solution by palm kernel fibre as sorbent, Dyes Pigm., 74 (2007) 60–66.
[53] S.F. Lütke, A.V. Igansi, L. Pegoraro, G.L. Dotto, L.A.A. Pinto, T.R.S. Cadaval Jr., Preparation of activated carbon from black wattle bark waste and its application for phenol adsorption, J. Environ. Chem. Eng., 7 (2019) 1–40.
[54] N. Mojoudi, N. Mirghaffari, M. Soleimani, H. Shariatmadari, C. Belver, J. Bedia, Phenol adsorption on high microporous activated carbons prepared from oily sludge: equilibrium, kinetic and thermodynamic studies, Sci. Rep., 9 (2019) 1–12.
[55] R. Ragadhita, A.B.D. Nandiyanto, How to calculate adsorption isotherms of particles using two-parameter monolayer adsorption models and equations, Indones. J. Sci. Technol., 6 (2021) 205–234.
[56] O. Hamdaoui, E. Naffrechoux, Modeling of adsorption isotherms of phenol and chlorophenols onto granular activated carbon: Part I. Two-parameter models and equations allowing determination of thermodynamic parameters, J. Hazard. Mater., 147 (2007) 381–394.
[57] R. Foroutan, S.J. Peighambardoust, S. Hemmati, A. Ahmadi, E. Falletta, B. Ramavandi, C.L. Bianchi, Zn^{2+} removal from the aqueous environment using a polydopamine/hydroxyapatite/Fe_3O_4 magnetic composite under ultrasonic waves, RSC Adv., 11 (2021) 27309–27321.
[58] A. Adak, A. Pal, M. Bandyopadhyay, Removal of phenol from water environment by surfactant-modified alumina through adsolubilization, Colloids Surf., A, 277 (2006) 63–68.
[59] P. Strachowski, M. Bystrzejewski, Comparative studies of sorption of phenolic compounds onto carbon-encapsulated iron nanoparticles, carbon nanotubes and activated carbon, Colloids Surf., A, 467 (2015) 113–123.
[60] Z. Gong, S. Li, W. Han, J. Wang, J. Ma, X. Zhang, Recyclable graphene oxide grafted with poly(N-isopropylacrylamide) and its enhanced selective adsorption for phenols, Appl. Surf. Sci., 362 (2016) 459–468.
[61] B. Abussaud, H.A. Asmaly, Ihsanullah, T.A. Saleh, V.K. Gupta, T. Laoui, M.A. Atieh, Sorption of phenol from waters on activated carbon impregnated with iron oxide, aluminum oxide and titanium oxide, J. Mol. Liq., 213 (2015) 351–359.
[62] I. Vázquez, J. Rodríguez-Iglesias, E. Marañón, L. Castrillón, M. Álvarez, Removal of residual phenols from coke wastewater by adsorption, J. Hazard. Mater., 147 (2007) 395–400.
[63] V.T. Trinh, T.M.P. Nguyen, H.T. Van, L.P. Hoang, T.V. Nguyen, L.T. Ha, X.H. Vu, T.T. Pham, T.N. Nguyen, N.V. Quang, X.C. Nguyen, Phosphate adsorption by silver nanoparticles-loaded activated carbon derived from tea residue, Sci. Rep., 10 (2020) 1–13.
[64] G.W. Kajjumba, S. Emik, A. Öngen, H. Kurtulus Özcan, S. Aydın, In: S. Edebali, Advanced Sorption Process Applications, Selçuk University, Turkey, 2019, pp. 1–19.
[65] J.H. Samat, N.N.M. Shahri, M.A. Abdullah, N.A.A. Suhaimi, K.M. Padmosoedarso, E. Kusrini, A.H. Mahadi, J. Hobley, A. Usman, Adsorption of acid blue 25 on agricultural wastes: efficiency, kinetics, mechanism, and regeneration, Air Soil Water Res., 14 (2021) 1–12.
[66] M.A. Salam, R.M. El-Shishtawy, A.Y. Obaid, Synthesis of magnetic multi-walled carbon nanotubes/magnetite/chitin magnetic nanocomposite for the removal of Rose Bengal from real and model solution, Ind. Eng. Chem., 20 (2014) 3559–3567.
[67] B.S. Chittoo, C. Sutherland, Adsorption using lime-iron sludge–encapsulated calcium alginate beads for phosphate recovery with ANN- and RSM-optimized encapsulation, J. Environ. Eng., 145 (2019) 1–18.
[68] Z. Shehu, W.L. Danbature, B. Magaji, Y.S. Yakubu, D. Balarak, Adsorption of phenol from wastewater using copper oxide supported on activated carbon obtained from coal: thermodynamics and kinetics studies, Chem. Sci. Eng. Res., 3 (2021) 16–23.
[69] P. Muthamilselvi, R. Karthikeyan, B.S.M. Kumar, Adsorption of phenol onto garlic peel: optimization, kinetics, isotherm, and thermodynamic studies, Desal. Water Treat., 57 (2016) 2089–2103.